

Probing the structure of a birthplace of intermediate-mass stars: Ammonia cores in Lynds 1340

M. Kun¹, J.G.A. Wouterloot², and L.V. Tóth^{3*}

¹ Konkoly Observatory, H-1525 Budapest, P.O.Box 67, Hungary

² Joint Astronomy Centre, 660 N. A'ohoku Place, University Park, 96720 Hilo, Hawaii, USA

³ Department of Astronomy, Loránd Eötvös University, H-1117 Budapest, Pázmány Péter sétány 1, Hungary

Received / Accepted

Abstract. Lynds 1340, a molecular cloud forming intermediate-mass stars, has been mapped in the NH₃(1,1) and (2,2) transitions with the Effelsberg 100-m telescope. We observed the whole area of the cloud where C¹⁸O emission was detected earlier, at a 40'' grid, with additional positions towards the C¹⁸O peaks and optically invisible IRAS point sources. Our observations covered an area of 170 arcmin², corresponding to about 5.15 pc² at a distance of 600 pc, and revealed 10 ammonia cores. The cores, occupying some 7% of the mapped area, probably represent the highest density regions of L 1340. Their total mass is ~80 M_⊙, about 6% of the mass traced by C¹⁸O. Six cores are associated with optically invisible IRAS point sources. Their average nonthermal line width is 0.78 km s⁻¹, while the same quantity for the four starless cores is 0.28 km s⁻¹. We suggest that the narrow-line cores are destined to form low-mass stars, whereas small groups of intermediate-mass stars are being formed in the turbulent cores. The features traced by NH₃, ¹³CO, C¹⁸O and H I obey the line width–size relation $\Delta v_{\text{NT}} \propto R_{1/2}^{0.41}$. Comparison of sizes, densities and nonthermal line widths of ammonia cores with those of C¹⁸O and ¹³CO structures supports the scenario in which core formation has been induced by turbulent fragmentation. The typical physical properties of the NH₃ cores of L 1340, $\langle R_{1/2} \rangle = 0.08$ pc, $\langle T_{\text{kin}} \rangle = 13.8$ K, $\langle \Delta v_{\text{total}} \rangle = 0.64$ km s⁻¹, and $\langle M \rangle = 9 M_{\odot}$ are close to those of the high-mass star forming Perseus and Orion B clouds.

Key words. ISM: star formation – ISM: molecules – ISM: clouds – ISM: individual objects: L 1340 – stars: formation

1. Introduction

Observations of nearby star forming regions have shown that high mass stars are born as members of dense clusters in massive molecular cloud cores, whereas small, cold cores give birth to one or a few solar type stars. The transition from isolated to clustered mode of star formation occurs in molecular clouds forming intermediate mass stars (Testi, Palla & Natta 1999). Molecular cores forming isolated low-mass stars and rich clusters differ from each other in structure, physical properties and evolution (e.g. Caselli & Myers 1995). Observations of various star forming regions are helpful in getting an unbiased view on the physical processes leading to a particular mode of star formation. We studied the structure of Lynds 1340, a medium-mass molecular cloud in order to compare the properties of this H Ae/Be star birthplace with well-studied star forming environments.

The star-forming molecular cloud Lynds 1340 is located in Cassiopeia, near (l,b)=(130,11), at a distance of 600 pc from the Sun (Kun et al. 1994, hereafter Paper I). In optical images, the cloud is visible as the faint, blue reflection nebula DG 9 (Dorschner & Gürtler 1966), which is illuminated by *B* and *A* type stars. RNO 7, 8 and 9 (Cohen 1980) associated with the cloud are probably signposts of recent star formation in L 1340.

Paper I presented ¹³CO and C¹⁸O maps of L 1340, obtained with the 4-m radio telescope of Nagoya University, its distance determination, and a list of candidate young stellar objects. The ¹³CO observations revealed a molecular mass of 1200 M_⊙, distributed in three clumps denoted as *cores A*, *B* and *C*, each associated with a number of IRAS point sources and H α emission stars. Following the definition given by Blitz & Williams (1999), however, it is more appropriate to refer to these ¹³CO substructures as *clumps*, which may contain higher density cores.

Yonekura et al.'s (1997) ¹³CO survey results have shown this cloud to be fairly isolated, instead of being a part of a giant molecular complex. They also pointed out that earlier Nagoya ¹³CO and C¹⁸O measurements cal-

Send offprint requests to: M. Kun e-mail: kun@konkoly.hu

* Present address: Max-Planck-Institut für Astronomie, Königstuhl 17, D-69117 Heidelberg, Germany

ibrated with S140, including those presented in Paper I, should be revised due to the incorrect value of 6 K used for the ^{13}CO radiation temperature of S140. (C^{18}O measurements were calibrated assuming the same ratio for T_R^*/T_A as that for the ^{13}CO line.) Using the revised value of 9 K, column densities and volume densities derived from the optically thin C^{18}O line can easily be corrected.

Recently, Kumar, Anandarao & Yu (2002) found three optical HH objects, HH 487, 488, and 489, emerging from YSOs in L 1340 A. The same work also has shown that RNO 7 is a compact cluster of some 26 stars, and predicted a mass about $6 M_\odot$ for its brightest member. Recent spectroscopic study of the illuminating stars of DG 9 and the candidate YSOs listed in Paper I suggests that L 1340 is a birthplace of small groups of low and intermediate mass stars (Kun 2002a). No O-type stars have been formed in this cloud. Both its size and star forming properties represent an intermediate mode between the isolated low mass star formation and clustered high mass star formation. Adams & Myers (2001) proposed that probably a significant part of field stars have formed in small groups consisting of less than a hundred members. Studies of star forming regions like L 1340 therefore add important pieces of information to the star formation history of our Galaxy.

In order to find the distribution of high density gas closely related to star formation, and its connection to the observed signposts of recent star formation we observed the (1,1) and (2,2) inversion lines of ammonia in regions of the cloud which have shown high column densities in the C^{18}O emission. The $\text{NH}_3(1,1)$ line is suitable for probing the density regimes around $n(\text{H}_2) \approx 10^4 \text{ cm}^{-3}$ (Harju, Walmsley & Wouterloot 1993, hereafter HWW). These densities are high enough to shield the gas from interstellar UV radiation, and thus disconnect them from the magnetic fields. Ammonia cores are those regions of the molecular clouds, where the self-similar structure resulted from interstellar turbulence breaks down and star formation becomes possible.

In this paper we present the results of the ammonia observations. On one hand, we expect to get a better view of the structure of the highest density parts of L 1340, owing to the higher angular resolution of our observations than those presented in Paper I. Comparison of physical parameters derived from NH_3 , C^{18}O and ^{13}CO observations, on the other hand, may reveal a relationship between different density regimes of the molecular gas. The ammonia database by Jijina, Myers & Adams (1999, hereafter JMA) makes it possible to compare L 1340 with other star forming regions. A spectroscopic and photometric follow-up study of the candidate YSOs associated with the cloud will be published in a subsequent paper (Kun 2002b).

We describe our ammonia observations in Sect. 2. The methods of our data analysis are presented in Sect. 3, and the results of observations in Sect. 4. In Sect. 5 we discuss the connection of ammonia cores with candidate YSOs and with their environment revealed by ^{13}CO , C^{18}O , H I and visual extinction. We also compare the dense cores of L 1340 with other star forming clouds. Sect. 6 gives a

brief summary of our results. Appendices A and B briefly outline how the use of publicly available H I and star count data contribute to get a coherent picture of the cloud.

2. Observations

We mapped the (1,1) and (2,2) inversion transition lines of ammonia towards L 1340 using the 100-m radio telescope of MPIfR at Effelsberg in February and October 1997. The half-power beam width of the telescope at 23.7 GHz is $40''$, corresponding to 0.12 pc at the distance of L 1340. The facility 1.3 cm maser receiver was used with a typical system temperature of 90 K. The spectrometer was a 1024-channel autocorrelator split into two bands of 6.25 MHz in order to observe simultaneously at the frequencies of $\text{NH}_3(1,1)$ (23694.495 MHz) and $\text{NH}_3(2,2)$ (23722.633 MHz). The spectral resolution was 0.15 km s^{-1} .

The mapping was done in total power mode with 3 ONs per OFF on a $40''$ grid, with additional positions towards the C^{18}O peaks and optically invisible IRAS point sources. The integration times were 3 minutes per position. We calibrated our measurements using continuum scans of NGC 7027 for which we adopted $T_{\text{MB}}=8.2 \text{ K}$, corresponding to 5.86 Jy (Baars et al. 1977). The pointing was checked each 2–3 hours on nearby continuum sources. Its accuracy was about $5''$. The typical rms noise in our spectra is 0.15 K (T_{MB}).

Our ammonia observations covered an area of 170 arcmin^2 , or 5.15 pc^2 at a distance of 600 pc. Virtually the whole area was observed where $\int T_A(\text{C}^{18}\text{O}) dv$ (Paper I) was higher than about 0.45 K km s^{-1} . Figure 1 shows the observed positions overlaid on the red optical image of L 1340 obtained from DSS-1¹.

3. Data analysis

3.1. Physical properties of the ammonia gas

Our ammonia spectra were reduced and analysed using the CLASS software (Forveille et al. 1989). We derived the physical parameters of the NH_3 gas following the procedure described by HWW. During this procedure we took into account the beam filling factor. It was estimated from the half-maximum sizes of the structures in the integrated intensity maps (Figs. 3–5, Sect. 4) and the HPBW of the telescope using Martin's & Barrett's (1978) Eq. 7. We obtained average beam filling factor of 0.5, which value we used in the data analysis.

¹ Based on photographic data of the National Geographic Society – Palomar Observatory Sky Survey (NGS-POSS) obtained using the Oschin Telescope on Palomar Mountain. The NGS-POSS was funded by a grant from the National Geographic Society to the California Institute of Technology. The plates were processed into the present compressed digital form with their permission. The Digitized Sky Survey was produced at the Space Telescope Science Institute under US Government grant NAG W-2166.

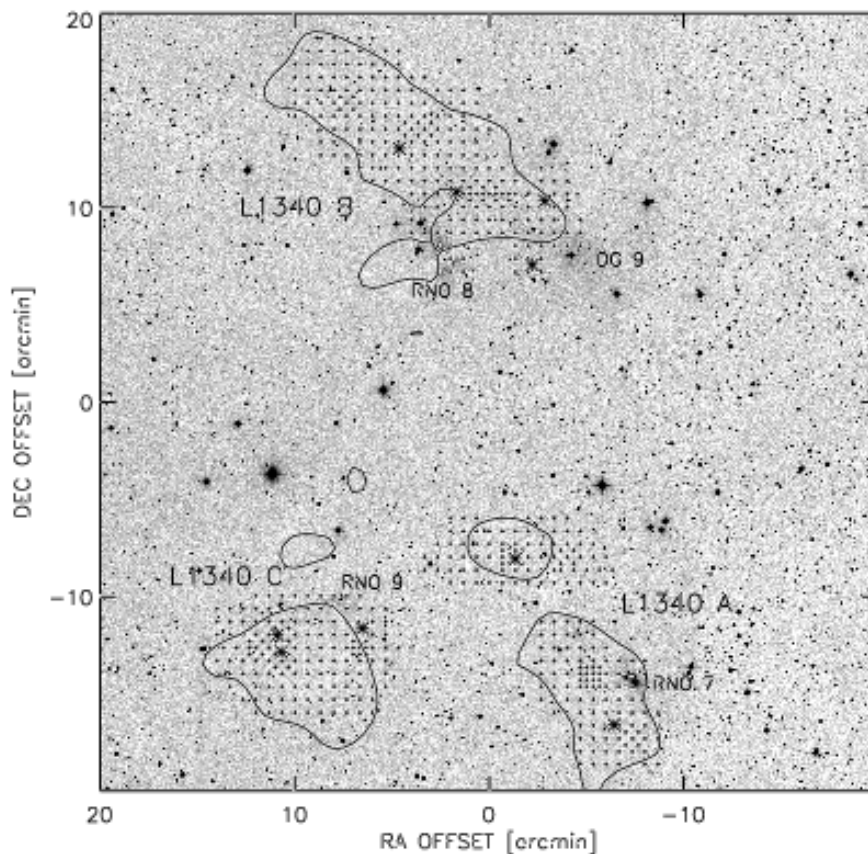


Fig. 1. The observed points (crosses) overlaid on the optical image of L 1340 taken from the DSS-1 red. The C^{18}O cores are indicated by their $\int T_A dv = 0.45 \text{ K km s}^{-1}$ contour. Asterisks show the positions of optically invisible and nebulous IRAS point sources. Positions of DG 9 and the RNOs are also indicated. Coordinate offsets are given in arcmin with respect to $\text{RA}(2000)=2^{\text{h}}30^{\text{m}}0$, $\text{D}(2000)=72^{\circ}52'0$.

The rotational temperature T_{12} can be determined from the (1,1) and (2,2) brightness temperatures (Ho & Townes 1983). At most positions of L 1340, however, the (2,2) line was too weak ($T_{\text{B}}(2,2) < 2\sigma$), therefore we averaged the (1,1) and (2,2) spectra for the regions around $T_{\text{B}}(1,1)$ maxima in order to enhance the S/N and determined T_{12} from the averaged spectra, using Ho & Townes (1983) Eq. 4. The T_{12} values were then transformed into kinetic temperatures T_{k} according to Walmsley & Ungerechts (1983), using collisional rate coefficients given by Danby et al. (1988).

The excitation temperature T_{ex} of the transition was determined where $T_{\text{B}}(1,1) > 5\sigma$, the signal-to-noise ratio allowed us to fit the (1,1) spectra with the pattern of the hyperfine components. We obtained excitation temperatures of 5–6 K for these positions, therefore we assumed $T_{\text{ex}} = 6 \text{ K}$ for the parts of the clouds where the S/N of the spectra was insufficient for the determination of T_{ex} .

The column density $N(\text{NH}_3(1,1))$ was computed using different assumptions depending on line intensities in accordance with the criteria given by HWW, and total ammonia column densities, $N(\text{NH}_3)$, were derived using HWW's Eq. 7.

3.2. Physical properties of ammonia cores

The distribution of $\text{NH}_3(1,1)$ integrated intensity shows several peaks, that define the positions of the dense cores of L 1340. We defined the ammonia cores as closed areas bordered by the lowest significant ($3\sigma = 0.45 \text{ K km s}^{-1}$) contours in the $\text{NH}_3(1,1)$ integrated intensity maps. Multiple peaks inside a closed contour are regarded as different cores if they are separated below the half-maximum contour. Table 1 shows the observed properties of the ammonia cores. The following quantities are listed: Column 1: the name of the core; Cols. 2–3: the offsets of the peak position of the integrated intensity in arcmin with respect to $\text{RA}(2000)=2^{\text{h}}29^{\text{m}}41^{\text{s}}64$ and $\text{Dec}(2000)=+72^{\circ}43'22''2$; Col. 4: the radial velocity obtained by fitting the NH_3 hyperfine structure to the observed spectra, averaged for the points within the border of the core, and its standard deviation; Col. 5: the average line width of the clump and its dispersion; This quantity was derived from the $\text{NH}_3(1,1)$ fit to the mean spectra, obtained by averaging individual spectra within the 3σ contour of the integrated intensity maps. Δv was corrected for the spectral resolution. Col. 6: the full angular size of the core within the 3σ contour of the integrated intensity map in arcsec, not corrected for

the beam size. We obtained this information by approximating the 3σ contour with an ellipse; Col. 7: the angular distance of the nearest IRAS source from the ammonia peak in arcsec; Col. 8: the name and type of the nearest IRAS source. An ‘s’ following the IRAS name marks sources associated with visible stars, and ‘i’ is for optically invisible sources.

In this section we describe the methods used for deriving sizes, kinetic temperatures, hydrogen column densities, masses, and nonthermal velocity dispersions of ammonia cores. We estimate their stabilities, and define their connection to IRAS point sources.

The *half-maximum radii* $R_{1/2}$ of the cores, corrected for the angular resolution of the observations were derived as $R_{1/2} = [A_{1/2}/\pi - (\text{HPBW}/2)^2]^{1/2}$, where $A_{1/2}$ was the area of the core within the half-maximum contour of the integrated intensity maps.

In order to determine the *mean kinetic temperatures* of the cores we averaged the (1,1) and (2,2) spectra over the positions within the lowest significant integrated intensity contours. The resulting spectra, due to their higher S/N made it possible to measure the integrated intensity of the (2,2) lines. Figure 2 shows the average spectra for cores A3, B1 and C3w.

Having estimates on the kinetic temperatures the *nonthermal line widths* of the cores can be determined: $\Delta v_{\text{NT}}^2 = \Delta v_{\text{obs}}^2 - 8 \ln 2 k T_{\text{k}} / m_{\text{obs}}$, where Δv_{NT} is the FWHM of the nonthermal (turbulent) motion, and $m_{\text{obs}} = 17 m_{\text{H}}$ is the mass of the ammonia molecule.

Hydrogen column densities $N(\text{H}_2)$ were calculated from ammonia column densities with the assumption that $\text{NH}_3/\text{H}_2 = n(\text{NH}_3)/n(\text{H}_2) = 3 \times 10^{-8}$, a mean value predicted by the models of chemical evolution of protostellar cores (Bergin & Langer 1997). According to the models NH_3/H_2 is constant during the protostellar collapse, but increases during the later evolution of cores, when shocks accompanying star formation release the molecules formed on grains (Nejad et al. 1990; Suzuki et al. 1992). For those positions of the cloud, where both T_{ex} and T_{k} were determined, $n(\text{H}_2)$ was derived independently of NH_3/H_2 (Ho & Townes 1983, Eq. 2). These positions allow us to check the adopted value of NH_3/H_2 when we make an assumption on the geometry of the cores.

Core masses were determined by summing up the mass elements $N(\text{H}_2) dx dy$ for each position with $N(\text{NH}_3) \geq 1.2 \times 10^{14} \text{ cm}^{-2}$, the lowest closed contour for most of the cores, and adding 20% helium (in number density). Here $N(\text{H}_2)$ is the hydrogen column density and $dx dy$ is the area corresponding to the grid spacing at a distance of 600 pc. We observed at a $40''$ grid, with several additional points halfway between two grid points, therefore we interpolated linearly the column densities so that we got a regular grid with spacing of $20''$.

In estimating the dynamical states of the ammonia cores their gravitational and kinetic energies, as well as the external pressure due to the weight of the overlying cloud have to be taken into account. Inserting the mass and radius of L1340 obtained from ^{13}CO

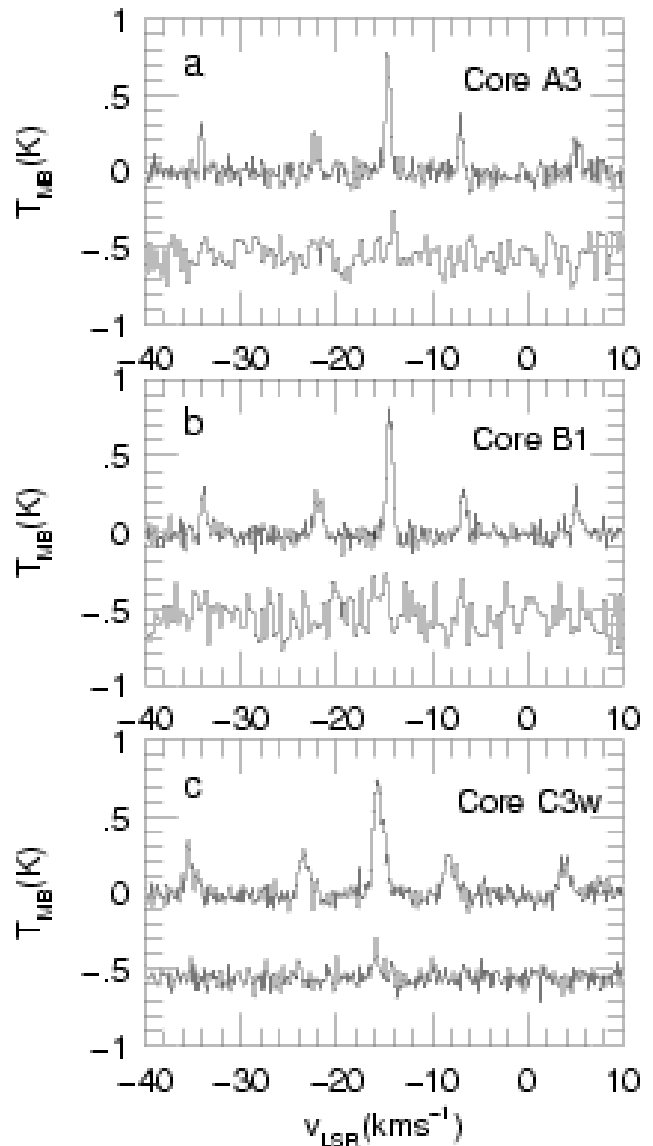


Fig. 2. Averaged spectra used for determining T_{12} for cores a) A3, b) B1, c) C3w.

data (Yonekura et al. 1997) into the formula $P_{\text{ext}}/k \approx 1.4(M/M_{\odot})^2(R/\text{pc})^{-4}$ (Bertoldi & McKee 1992) resulted in the mean external pressure $P_{\text{ext}}/k \approx 2.4 \times 10^5 \text{ K cm}^{-3}$. With this data we estimated the critical Bonnor–Ebert mass of the cores, $M_{\text{BE}} = 1.18 \sigma^4 / (G^3 P_{\text{ext}})^{1/2}$, where $\sigma^2 = \Delta v^2 / 8 \ln 2$, and G is the gravitational constant. Cores more massive than M_{BE} will collapse to form stars in this environment, if other effects are neglected.

3.3. Connection of cores with YSOs

Optically invisible IRAS point sources projected on the cores are supposed to be embedded YSOs born in the cores. We associate an embedded YSO with a core, following JMA, if it lies within $2 \times R_{1/2}$ to the peak of the core. Connection of optically visible YSOs with the cores

Table 1. Measured parameters of NH₃ cores of L 1340

Core	RA offset ($'$)	D offset ($'$)	v_{LSR} (km s^{-1})	Δv (km s^{-1})	Ang. size ($" \times "$)	d(*) "	Nearest IRAS source
A1	-6.00	-8.33	-14.13 (0.03)	0.64 (0.06)	140×60	60	02238+7222 <i>i</i>
A2	-4.00	-5.33	-14.35 (0.03)	0.36 (0.04)	80×20		
A3	-2.33	0.00	-14.56 (0.01)	0.28 (0.02)	70×60		
A4	0.33	0.33	-13.75 (0.30)	0.99 (0.08)	90×60	10	02249+7230 <i>i</i>
B1	2.33	19.67	-14.37 (0.15)	0.63 (0.03)	85×70	40	F02256+7249 <i>i</i>
B2	4.00	20.00	-14.67 (0.03)	0.29 (0.05)	90×40	68	
C1	8.33	-4.33	-14.63 (0.09)	0.67 (0.04)	100×70	80	02267+7226 <i>i</i>
C2	12.33	-3.00	-15.89 (0.14)	0.84 (0.04)	80×70	20	F02277+7226 <i>i</i>
C3w	12.67	-4.67	-15.71 (0.36)	0.97 (0.05)	100×60	50	02276+7225 <i>i</i>
C3e	13.67	-4.00	-15.92 (0.10)	0.40 (0.03)	80×50	40	F02279+7225 <i>s</i>

is less obvious. These more evolved objects may either have been born in the core on which they are projected or in another core which has already dispersed. In the following discussions we shall assume the cores having optically identified IRAS point sources or H α emission stars within $2 \times R_{1/2}$ to their peak $T_B(1,1)$ to be starless. Our classification is somewhat uncertain because, due to the large distance of L 1340, only the most luminous members of the YSO population were detected by IRAS. Most IRAS sources in L 1340 are faint, close to the detection threshold, have less than four good quality fluxes, and are extended in the 100 μm image. We note that only one optically invisible source, IRAS 02249+7230 has a good flux quality at 100 μm .

4. Results

4.1. Distribution of ammonia in L 1340

The ammonia cores defined by the integrated intensity distribution of the main-group of the (1,1) line are shown in the left panels of Figures 3–5 for clumps *A*, *B*, and *C*, respectively. For comparison, we also plotted the C¹⁸O contours $\int T_A dv = 0.45 \text{ K km s}^{-1}$ and 0.75 K km s^{-1} . The ammonia cores are labelled in the figures.

In addition to the cores defined in Sect. 3.2 there is an extended region of weak NH₃(1,1) emission in the northern part of clump *B*, around the position of the C¹⁸O peak. The integrated intensity of the (1,1) line is below the 3σ limit at most positions. The optically invisible source IRAS 02263+7251 lies in this area. Averaging 56 spectra around the position the C¹⁸O peak (bordered by a dotted polygon in Fig. 4) we obtained the spectrum displayed in Fig. 6. The weak line indicates low average column density for this region. Because the critical density of the excitation of NH₃(1,1) emission is about 10^4 cm^{-3} , this part of the cloud probably contains high density regions much smaller than the angular resolution of our observations.

Column density maps are shown in the right panels of Figs. 3–5. IRAS point sources associated with the cores are

labelled in these figures. Because of the effect of the optical depth, column densities are not directly proportional to the integrated intensities. Comparison of the two sets of maps shows the main structures to be largely similar, with the exception that core *C3* splits into two parts, *C3w* and *C3e*, in the column density map.

The physical properties of the cores, derived by the procedures described in Sect. 3.2, are displayed in Table 2. The following quantities are listed: Col. 1: name of the core. An asterisk following the name indicates that we associated the core with an embedded YSO; Col. 2: the half-maximum radius $R_{1/2}$, in parsecs; Col. 3: T_{ex} at the peak position where the S/N of the line allowed its determination; Col. 4: the mean kinetic temperature T_k ; Col. 5: the nonthermal component of the line width Δv_{NT} ; Col. 6: the maximum column density $N_{\text{max}}(\text{NH}_3)$; Col. 7: volume density $n(\text{H}_2)$ of the hydrogen derived from T_{ex} ; Col. 8: the mass of the core in solar masses. The Bonnor–Ebert mass is shown in Col. 9. Bolometric luminosity of the optically invisible IRAS point source associated with the core, calculated from the IRAS fluxes adding the long-wavelength bolometric correction (Myers et al. 1987) is shown in Col. 10. Where only flux upper limits were available, we estimated the fluxes from the infrared data sets (IRDS) obtained via the *IRAS Software Telescope* maintained at SRON (Assendorp et al. 1995).

The observed ammonia cores probably represent the densest regions of L 1340. *B1* and *B2*, as well as *C3w* and *C3e* constitute twin core systems according to the definition by JMA. The cores are located close to the C¹⁸O peaks in clump *A* within the accuracy set by the different angular resolutions. In clumps *B* and *C*, however, the high density regions indicated by the ammonia emission are located far from the column density peaks of the C¹⁸O. These small dense regions might have been missed during the C¹⁸O survey because of their half-maximum sizes are smaller than the grid spacing ($2'$). The total mass in the dense cores is $79 M_{\odot}$, some 6% of the mass traced by C¹⁸O.

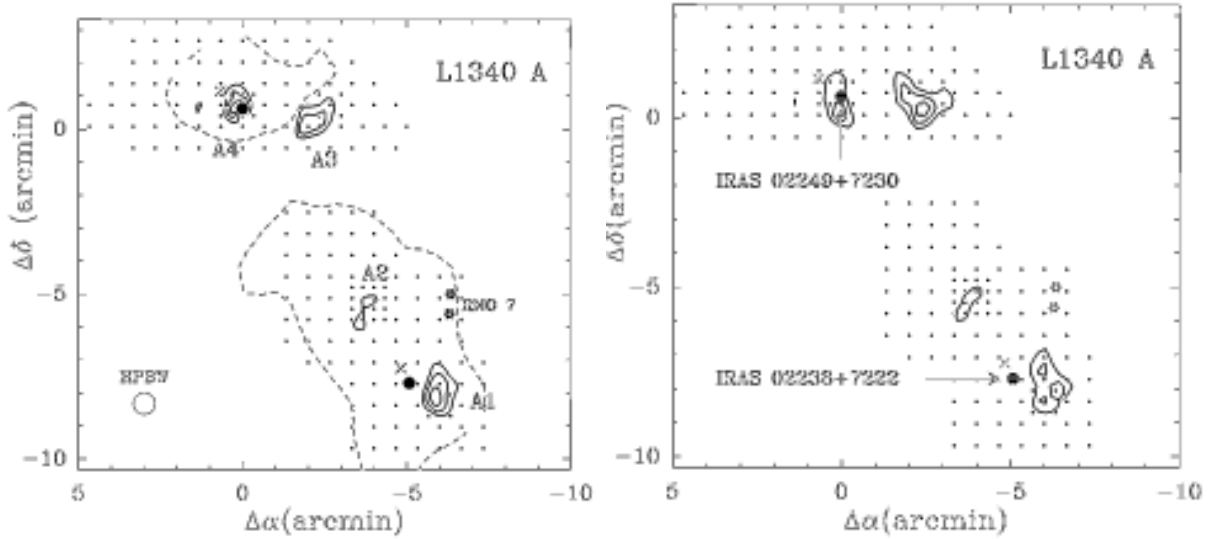


Fig. 3. *left:* $\text{NH}_3(1,1)$ (solid contours) main group integrated intensity map of L 1340 A. The emission was integrated over the velocity interval between -17 km s^{-1} and -12 km s^{-1} . The lowest contour is 0.40 K km s^{-1} , and the increment is 0.15 K km s^{-1} . The observed positions are shown by dots. Black circles mark the positions of optically invisible IRAS point sources, and asterisks indicate those associated with visible stars. Crosses show the positions of the C^{18}O peaks. Dashed contours indicate the 0.45 K km s^{-1} level of the $\int \text{C}^{18}\text{O } dv$ distribution. The HPBW of the ammonia observations is shown in the lower left corner. The HPBW of the C^{18}O was $2'.7$. Coordinate offsets are given in arcmin with respect to $\text{RA}(2000)=2^{\text{h}}29^{\text{m}}41^{\text{s}}.64$ and $\text{Dec}(2000)=+72^{\circ}43'22''.2$. *right:* Ammonia column density map of L 1340 A. The lowest contour is at $1.2 \times 10^{14} \text{ cm}^{-2}$, and the increment is $0.6 \times 10^{14} \text{ cm}^{-2}$.

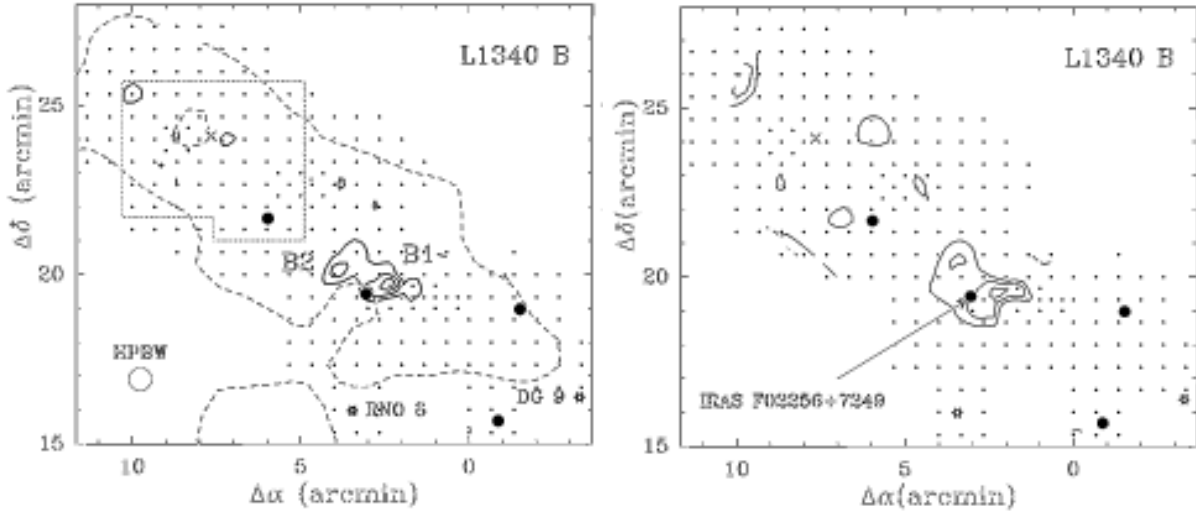


Fig. 4. Same as Fig. 3, but for L 1340 B. *left:* Contours start at 0.40 K km s^{-1} , and the increment is 0.20 K km s^{-1} . The polygon drawn by dotted line indicates an extended region where weak emission ($T_{\text{B}}(\text{NH}_3(1,1)) \leq 2\sigma$) was detected. *right:* The lowest contour is at $1.2 \times 10^{14} \text{ cm}^{-2}$, and the increment is $0.4 \times 10^{14} \text{ cm}^{-2}$.

4.2. Velocity structure

While neither C^{18}O nor NH_3 observations have indicated velocity gradients in L 1340 A and L 1340 B, C^{18}O measurements of L 1340 C have shown a clear radial velocity gradient of $0.71 \text{ km s}^{-1} \text{ pc}^{-1}$ in the galactic longitude direction, which was interpreted as rotation of the clump in Paper I. The ammonia data, having higher angular resolution, suggest another possible scenario. Figure 3 shows

that clump C contains two high density regions, separated by a lower density region between the right ascension offsets of about $9'.16$ and $10'.83$. The two subclumps have a velocity difference of about 1.2 km s^{-1} (Table 2). The observed velocity gradient may result from the overlapping of the two clumps of different radial velocities. A similar situation was found in Orion KL by Wang et al. (1993).

Figure 7a displays v_{LSR} as a function of $\Delta\alpha$, at several δ offsets. The less negative velocity component at

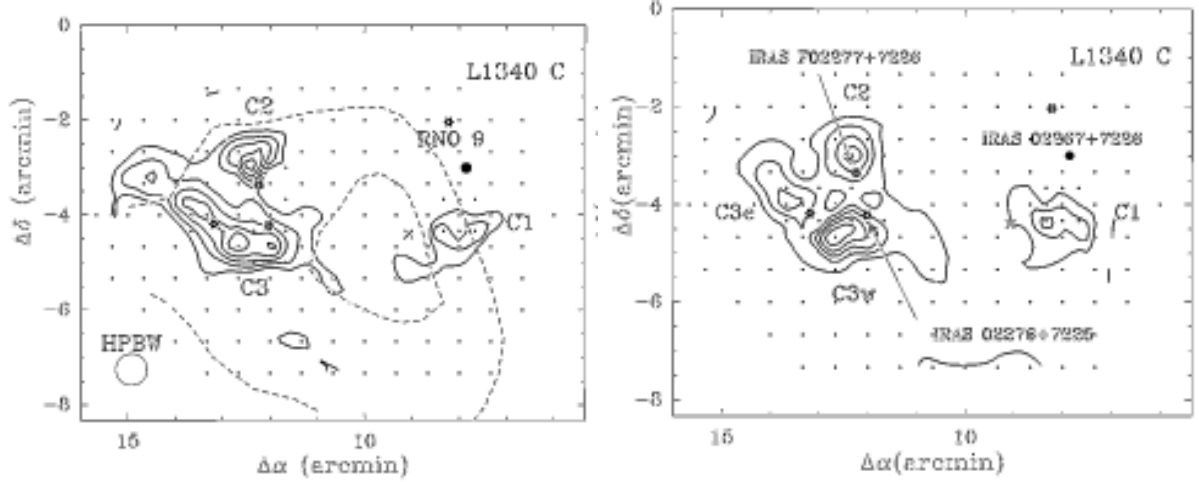


Fig. 5. Same as Fig. 3, for L 1340 C. *left:* Contours start at 0.45 K km s^{-1} , and the increment is 0.20 K km s^{-1} . Due to the larger velocity range observed in this clump the emission was integrated over the velocity interval of -19 km s^{-1} – -12 km s^{-1} . *right:* The lowest contour is at $1.2 \times 10^{14} \text{ cm}^{-2}$, and the increment is $0.8 \times 10^{14} \text{ cm}^{-2}$.

Table 2. Derived physical parameters of the NH_3 cores of L 1340

Core	$R_{1/2}$	T_{ex}	T_{k}	Δv_{NT}	$N_{\text{max}}(\text{NH}_3)$	$n(\text{H}_2)$	$M(\text{NH}_3)$	M_{BE}	L_{IRAS}
	(pc)	(K)	(K)	(km s^{-1})	(10^{14} cm^{-2})	(10^4 cm^{-3})	(M_{\odot})		(L_{\odot})
A1*	0.08	...	15.2 (2.0)	0.61	2.34 (0.24)	...	5.8	3.2	≤ 9.6
A2	0.04	...	≤ 12.5	0.31	2.10 (0.50)	...	1.5	0.4	
A3	0.08	4.7	11.9 (2.3)	0.21	3.40 (0.33)	0.99 (0.08)	6.5	0.2	
A4*	0.06	...	13.5 (2.0)	0.97	2.53 (0.60)	...	3.7	18.6	4.9
B1*	0.10	5.2	14.6 (3.1)	0.67	2.05 (0.27)	1.44 (0.10)	5.6	3.0	8.8
B2	0.08	...	≤ 15.0	0.24	1.45 (0.40)	...	2.7	0.2	
C1*	0.10	4.7	14.1 (1.7)	0.64	3.57 (0.46)	...	12.0	3.9	2.8
C2*	0.10	4.6	16.7 (1.6)	0.81	4.61 (0.60)	1.07 (0.18)	10.2	9.7	...
C3w*	0.15	5.2	13.6 (1.1)	0.95	4.89 (1.50)	1.82 (0.40)	15.6	17.2	1.5
C3e	0.11	6.0	12.5 (4.0)	0.36	3.73 (0.57)	1.29 (0.36)	15.4	0.5	
Mean	0.08	5.1	14.0	0.58	3.07	1.32	7.9	5.7	5.4
Starless cores	0.07	5.1	12.2	0.28	2.67	1.14	6.5	0.3	...
Cores with stars	0.09	5.0	14.6	0.78	3.33	1.44	8.8	9.3	5.4

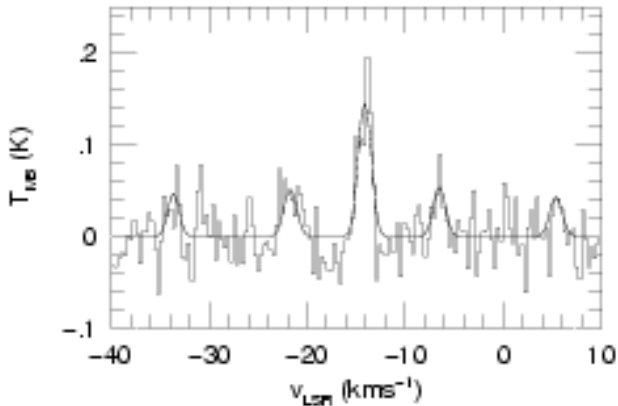


Fig. 6. Average of 56 $\text{NH}_3(1,1)$ spectra in the region centered on the C^{18}O peak position of clump B.

$\Delta\alpha < 11'$ shows a small velocity gradient. The velocity changes abruptly between the offsets $11'33$ and $12'00$, and is nearly constant (about -15.6 km s^{-1}) at larger offsets. Both components can be observed at $11'33 \leq \Delta\alpha \leq 13'33$. This overlapping shows up as an increase in the line widths in this $\Delta\alpha$ interval (Fig. 7b). The region of enhanced line widths coincides with the part of the clump where IRAS point sources are found. This morphology suggests that clump collision might have played role in triggering star formation in L 1340 C.

5. Discussion

Ammonia cores are those regions of the interstellar medium where the volume density is between 10^4 – 10^5 cm^{-3} . In respect of physical properties they do not form a homogeneous group. Starless cores in most clouds

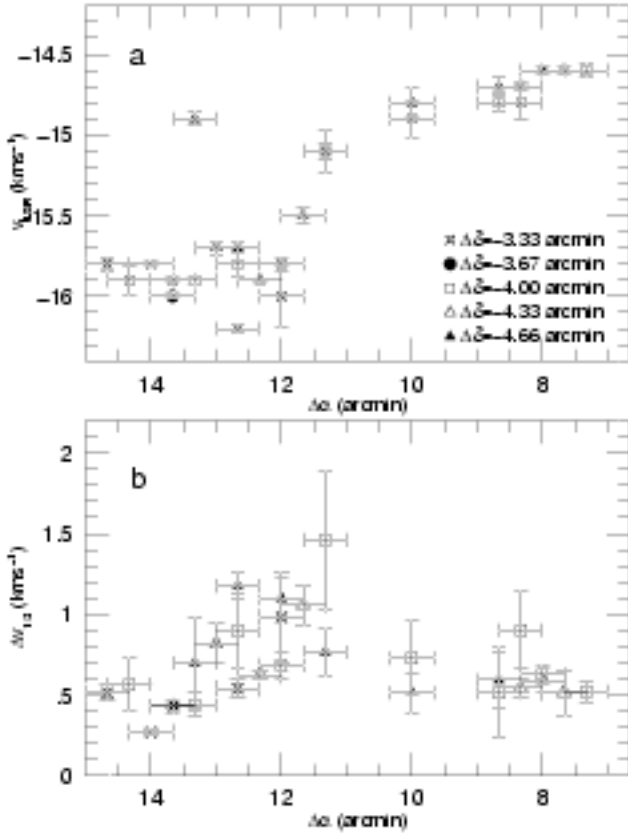


Fig. 7. a) Radial velocities in Clump C as a function of RA offset; b) Linewidths observed in Clump C as a function of RA offset. Different declination offsets are marked with different symbols. Offsets are given in arcmin with respect to RA(2000)=2^h29^m41^s.64 and Dec(2000)=+72°43′22″.2.

have smaller nonthermal line widths and masses, and lower kinetic temperatures than those associated with IRAS sources. Moreover, the cores associated with embedded or nearby young clusters are the most massive and most turbulent objects in JMA’s ammonia data base. The typical mass and turbulent energy of gas in the cores, moreover, varies from cloud to cloud. Most cores in Taurus form isolated stars, whereas some of them in Ophiuchus and Orion give birth to rich clusters (Motte et al. 1998; Mitchell et al. 2001). Several observational and theoretical studies suggest that the observed nonthermal line widths of cores are related to the initial conditions of star formation (e.g. Myers & Fuller 1993; Caselli & Myers 1995).

Dense cores of molecular clouds are thought to be created by shocks due to the supersonic turbulent velocity field of the ISM, referred to as turbulent fragmentation (e.g. Elmegreen 1993; Klessen, Heitsch & Mac Low 2000). In this scenario several observed properties of core/cloud systems are related to the nature of interstellar turbulence (Padoan 1995; Padoan & Nordlund 2002). In particular, the slope α of the line width–size relation $\log \Delta v_{NT} \propto \alpha \log R$ reflects the power spectrum of the tur-

bulence, so that $E(k) \propto k^{-\beta}$ and $\alpha = (\beta - 1)/2$. Density ratio between cores and their environment, typical core diameter and mass, as well as the volume filling factor of the cores are related to the size L_0 and velocity dispersion $\sigma_{v,0}$ of the ambient cloud.

Cores of various size and velocity dispersion probably define the smallest scale of the self-similar structure of interstellar medium. In low-mass star forming regions they represent the size scale where the nonthermal velocity dispersion becomes subsonic (Goodman et al. 1998). Myers (1998) has shown that the strongly turbulent, massive cores having $\Delta v > 0.9 \text{ km s}^{-1}$ and $N(\text{H}_2) > 1 \times 10^{22} \text{ cm}^{-2}$ may contain several critically stable condensations (kernels) cut off from MHD waves due to the high extinction of the core. This model suggests that massive, cluster-forming cores also represent an inner scale of the self-similar structure.

In this section we attempt to deduce some attributes of star formation from the derived properties of ammonia cores of L1340 (Sect. 5.1), compare the features revealed by different tracers with each other (Sect. 5.2), and L1340 with other star forming regions (Sect. 5.3).

5.1. Connection of ammonia cores with star formation

Table 2 shows that $M(\text{NH}_3) \geq M_{BE}$ for most of the cores of L1340. Several observations have shown that this is a necessary condition of star formation (Williams et al. 2000). Thus the observed cores probably highlight the positions of present and future star formation. The cores associated with embedded YSOs clearly differ from the starless cores in their nonthermal line widths. This is also true for the twin systems. The mean Δv_{NT} of cores without embedded or nearby IRAS point source, 0.28 km s^{-1} , corresponds to a velocity dispersion $\sigma_{NT} = 0.12 \text{ km s}^{-1}$. This is smaller than the isothermal sound speed at 13 K, $c_s = 0.21 \text{ km s}^{-1}$. Thus the detected starless cores are among the smallest clumps formed by turbulent fragmentation. Such objects may have a wide range of mass (e.g. Padoan & Nordlund 2002), including small clumps which do not collapse. The weak ammonia emission observed at the northern part of clump B probably originates from such small, dense regions. $M(\text{NH}_3) \gg M_{BE}$ for the starless cores, indicating that they are destined to collapse. Our observations thus suggest that these cores are prestellar. We note, however, that this conclusion has some uncertainties. First, magnetic fields, neglected here due to lack of data, may modify the critical mass so that it will be significantly larger than M_{BE} . Furthermore, recent results by Tafalla et al. (2002) demonstrate that ammonia abundance is enhanced towards the centres of some starless cores. Detection of the central regions only, enriched in ammonia, may lead to overestimation of the mass. Finally, it is possible that these cores are not starless, but contain low-luminosity embedded YSOs below the detection threshold of IRAS. Observations in other molecular lines with high angular resolution and more sen-

sitive infrared observations can clarify the nature of these cores.

Cores associated with embedded IRAS sources have average $\Delta v_{\text{NT}} = 0.78 \text{ km s}^{-1}$, comparable to the those of Orion B (JMA). From the six cores, column density and nonthermal line width of *A4* and *C3w* fulfil the criteria set by Myers (1998) for cluster forming cores. In core *A4* IRAS 02249+7230 closely coincides with the peak intensity of C^{18}O , NH_3 and A_V . $M_{\text{BE}} \gg M(\text{NH}_3)$ for this core, suggesting that it is disrupting. Morphology of HH 489, associated with the IRAS source, however, indicates that the direction of the bipolar outflow from this star lies close to the plane of the sky (Kumar et al. 2002). The large nonthermal velocity dispersion of this core thus cannot arise from the interaction of outflow with the core gas. It indicates either the presence of other YSOs with outflows along the line of sight, or might have been produced before the star formation. The other cluster-forming core candidate, *C3w*, has a common envelope with *C2* and *C3e*. Our ammonia observations show this core to be the densest region of L 1340, though it lies far from the C^{18}O peak, and is associated with a single low-luminosity IRAS source IRAS 02276+7225. No outflow, maser source or HH-object have been detected around this source. Core *C3w* is probably less evolved than *A4*.

Our observational results suggest that the large turbulent velocity dispersions of IRAS-associated cores cannot be attributed to YSO winds. These cores are not simply more evolved versions of the starless cores, but probably form more massive stars than their narrow-line counterparts, and some of them will evolve into small stellar groups similar to the two sparse young clusters RNO 7 and RNO 8, found in L 1340 (Kumar et al. 2002; Kun 2002a). In order to reveal the real nature and evolutionary state of the cores, their detailed density and velocity structures and stellar contents have to be studied via higher resolution molecular and submillimeter continuum observations.

5.2. Comparison with HI , ^{13}CO , C^{18}O , and A_V

The nonthermal line width–size relation for the structures shown by different tracers, called *Type 3 line width–size relation* by Goodman et al. (1998), is a useful indicator of the overall density structure of a cloud, which, in turn, is closely related to the mode of star formation. In order to derive this relation for L 1340 we supplemented our ammonia results with C^{18}O , ^{13}CO and HI data.

The Δv_{NT} and R data for the C^{18}O and ^{13}CO structures were taken from Paper I and from Yonekura et al. (1997), respectively. The size and line width of the HI structure associated with L 1340 were estimated from the Leiden–Dwingeloo HI survey data (Hartmann & Burton 1997). The main properties of the neutral hydrogen in the galactic environment of L 1340 are shown in Appendix A. The HI spectra in this region show definite peaks in the velocity interval $-18 \text{ km s}^{-1} < v_{\text{LSR}} < -8 \text{ km s}^{-1}$ whose characteristic FWHM is 7 km s^{-1} , and

the half-maximum size of the interstellar feature delineated by this gas component is 38 pc.

The $\log \Delta v_{\text{NT}}$ vs. $\log R$ relation for the structures observed in NH_3 , C^{18}O , ^{13}CO and HI is shown in Fig. 8. The $R_{1/2}$ values plotted have been corrected for the different beam sizes of the observations, and Δv_{NT} values have been corrected for spectral resolutions. We obtained the relation

$$\log \Delta v_{\text{NT}} = (0.41 \pm 0.06) \log R + (0.12 \pm 0.06) \quad (1)$$

and the correlation coefficient 0.85.

This relationship reveals the self-similar hierarchy of substructures from the large HI cloud to the ammonia cores, i.e. on the 0.1–40 pc size scale, suggesting that they are parts of a physically connected structure shaped by interstellar turbulence (Larson 1981). The slope $\alpha = 0.41$ is between those obtained for Taurus (0.53 ± 0.07) and Orion B (0.21 ± 0.03) cores (Caselli & Myers 1995), from the same tracers.

We compare properties of NH_3 cores and their embedding C^{18}O clumps in Table 3. The data listed show that the average density ratio of the cores and their embedding clumps n_c/n_0 , the typical core diameter l_c and the volume filling factor of the cores are in accordance with the values predicted by the model of turbulent fragmentation (Padoan 1995; Padoan & Nordlund 2002). The size and velocity dispersion of the ^{13}CO cloud are $L_0 = 3.7 \text{ pc}$ and $\sigma_{v,0} = 0.72 \text{ km s}^{-1}$, respectively, thus the large-scale Mach number is $\mathcal{M}_0 = \sigma_{v,0}/c_s = 3.4$. With these values the model gives $n_c/n_0 \approx \mathcal{M}_0^2 = 11.6$, in accordance with the observed $n_c/n_0 \approx 10$. The typical core diameter, $l_c \sim L_0 \mathcal{M}_0^{-1/\alpha} = 0.25 \text{ pc}$, is also comparable to the observed average 0.16 pc. The volume filling factor of the cores, obtained from the probability density function of n_c/n_0 , is 0.02, compatible with the observed average shown in Table 3.

Finally, in Fig. 9 we compare different density cross sections of L 1340, traced by ^{13}CO , C^{18}O , and NH_3 , with the distribution of total column density shown by the visual extinction A_V . Visual extinction map was constructed from star counts using the USNOFS Image and Catalogue Archive² (see Appendix B for the details of obtaining A_V). The angular resolution of ^{13}CO , C^{18}O and A_V maps is equally $3''$. Positions of ammonia cores, embedded YSOs and RNOs are also indicated. The amount of the foreground extinction was estimated and subtracted from the A_V values obtained from the star counts (see Appendix B). The three clumps can be recognized in the distribution of A_V , but some remarkable differences can also be seen between the structures shown by the obscuring dust and molecular gas. At the southwestern edge of the cloud, in clump *A*, similarity of ^{13}CO and A_V suggests that the total amount of A_V originates from the observed molecular gas. The steep gradients of both the column density

² Operated by the United States Naval Observatory, Flagstaff Station (<http://www.nofs.navy.mil/data/fchpix/>).

Table 3. Comparison of C¹⁸O and NH₃ cores in L 1340

Clump	A	B	C	Mean
$R(\text{C}^{18}\text{O}) / \text{pc}$	0.9	1.1	0.7	0.9
$\langle R \rangle(\text{NH}_3) / \text{pc}$	0.07	0.13	0.09	0.10
$\Delta v_{\text{tot}}(\text{C}^{18}\text{O})^a / \text{km s}^{-1}$	0.89	1.25	2.16	1.43
$\langle \Delta v_{\text{tot}} \rangle(\text{NH}_3)$	0.57	0.46	0.72	0.58
$T_{\text{ex}}(^{12}\text{CO}) (\text{K})$	10.2	13.1	9.2	10.8
$\langle T_k \rangle(\text{NH}_3) / \text{K}$	12.9	14.6	14.2	13.9
$N_{\text{H}_2}(\text{C}^{18}\text{O})^b / 10^{21} \text{cm}^{-2}$	7.1	8.4	7.8	7.8
$N_{\text{H}_2}(\text{NH}_3) / 10^{21} \text{cm}^{-2}$	8.6	6.8	14.0	9.8
$n_{\text{H}_2}(\text{NH}_3)/n_{\text{H}_2}(\text{C}^{18}\text{O})$	7.7	11.6	10.0	9.8
$\text{Area}(\text{NH}_3)/\text{Area}(\text{C}^{18}\text{O})$	0.04	0.02	0.16	0.07
$M_{\text{cores}}/M_{\text{clump}}$	0.04	0.02	0.19	0.08
$V_{\text{cores}}/V_{\text{clump}}$	0.01	0.002	0.11	0.04

^a The total line width, Δv_{tot} of a C¹⁸O core was calculated from the mean line width $\langle \Delta v \rangle$ obtained by averaging for each observed position within the half-maximum contour of the integrated intensity map and from the dispersion of the mean velocity (δv_{LSR}): $\Delta v_{\text{tot}}^2 = \langle \Delta v \rangle^2 + 8 \ln 2 (\delta v_{\text{LSR}})^2$.

^b taking into account the revised calibration (Yonekura et al. 1997).

and volume density suggest that the gas in this volume has suffered compression from an external shock. Both in Clump *B* and *C* large dark patches can be seen which do not correlate with the molecular emission (e.g. around offsets [14', -8'], [-4', 20']). These features indicate diffuse or overlapping clumps of high total column density. Together with the compact clump *A* they give asymmetric, cometary shape to the cloud with a ‘head’ pointing towards southwest. Surface distribution of the ammonia cores suggests that they have been formed by external compression or magnetic fields instead of gravity. Most of them (*A1*, *A2*, *B1*, *C1*, *C3*) are found far from the bottom of the gravitational potential well of the embedding clumps, indicated either by the peaks of the C¹⁸O intensity or by the large-scale distribution of A_V .

5.3. Comparison with other clouds

Comparison of properties of ammonia cores in L 1340 with JMA’s data base (their Tables B9–B20) shows that the typical sizes, kinetic temperatures, line widths and masses of ammonia cores are increasing in the order of Taurus → Ophiuchus → Perseus → L 1340 → Orion B → Orion A. The IRAS luminosities do not show this trend, being lower in L 1340 than in Perseus. A reason for this departure from the trend may be the difference in cloud distances. L 1340 is the most distant among the clouds listed above, therefore a considerable fraction of YSOs born in it might remained undetected by IRAS. We have shown in Sect. 5.2 that the slope α of the line width–size relation also shows the Taurus → L 1340 → Orion B trend, suggesting that

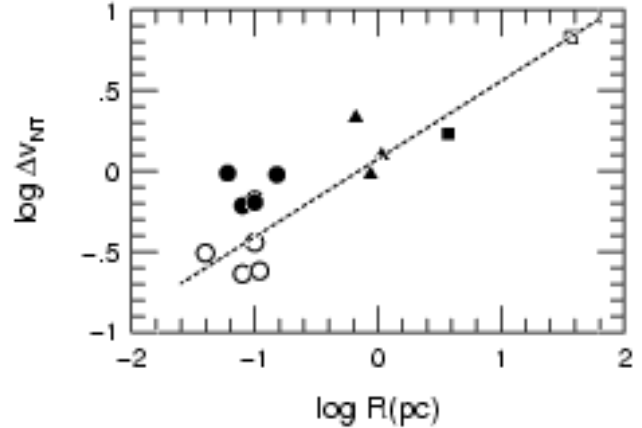


Fig. 8. The nonthermal line width–size relation for different substructures (ammonia cores, C¹⁸O clumps and the whole ¹³CO cloud) of L 1340. Open circles mark the starless NH₃ cores and those associated with optically visible stars, black circles represent the cores associated with IRAS point sources. Triangles are for the C¹⁸O clumps, and black square marks the whole ¹³CO cloud. The open square shows the H I feature, whose half-maximum size was estimated from Fig. A.2, and in estimating the non-thermal line width a kinetic temperature 80 K was assumed. The dashed line is fitted to all points.

properties of cores and newborn stars are related to large-scale interstellar processes. Comparison of observational results with the continuously improving numerical simulations of such processes will lead to a better understanding of the cloud formation and evolution. This is, however, beyond the scope of the present paper.

6. Summary of the results

The main results of ammonia observations of L 1340 are summarized as follows.

- (i) Mapping of the whole area of the cloud where C¹⁸O emission indicated high gas volume density ($n \geq 10^3 \text{cm}^{-3}$) in the NH₃(1,1) and (2,2) lines resulted in the detection of 10 dense cores in L 1340. We found the embedding cores of six candidate YSOs, namely IRAS 02238+7222, 02249+7230, F02256+7249, 02267+7226, 02276+7225 and F02277+7226. An additional object, IRAS 02263+7251 is associated with weak ammonia emission near the detection limit.
- (ii) $M > M_{\text{BE}}$ for most cores, indicating that they are able to form stars.
- (iii) The cores with and without embedded YSOs differ from each other in nonthermal line width. The non-thermal velocity dispersion is subsonic in the starless group. Outflows from the known embedded protostars cannot account for the high Δv_{NT} values of cores associated with IRAS sources. Therefore the two groups

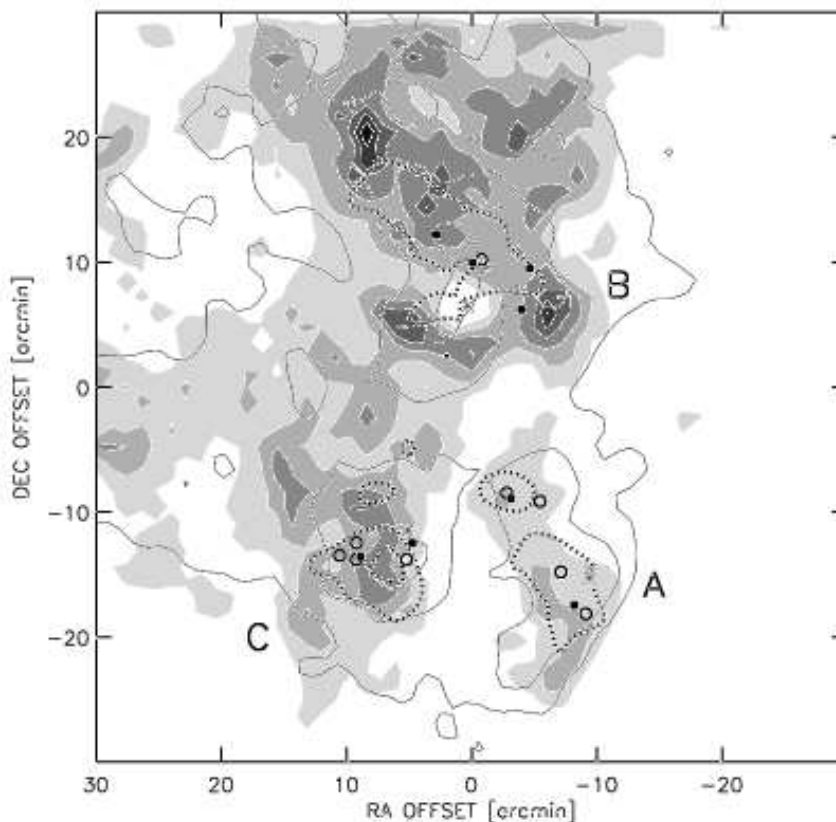


Fig. 9. ^{13}CO (solid contours) and C^{18}O (dotted contours) integrated intensity overlaid on the optical extinction map (shading) of L 1340 constructed from star counts. Coordinate offsets are given in arcmin with respect to $\text{RA}(2000)=2^{\text{h}}29^{\text{m}}42^{\text{s}}$ and $\text{Dec}(2000)=+72^{\circ}43'22''$. The lowest contour of ^{13}CO is at 1.0 K km s^{-1} , and the increment is 1.5 K km s^{-1} . The C^{18}O contours displayed are 0.45 and 0.75 K km s^{-1} . Both the lightest shade and the increment is 1 mag . The A_V values displayed are corrected for the foreground extinction. Open circles indicate the ammonia cores, which probably represent the regions of highest volume densities. Dots are optically invisible IRAS point sources, and asterisks show the positions of the RNOs.

differ from each other not only in evolutionary state. The nonthermal line width of cores is probably related to the masses of stars being formed in them.

- (iv) The velocity structure of L 1340 C revealed two clumps moving with supersonic velocities with respect to each other. Star formation has possibly been triggered by clump collision in this region.
- (v) The relations between the physical properties of NH_3 cores and the ^{13}CO and C^{18}O clumps are consistent with the scenario of turbulent fragmentation.
- (vi) The nonthermal line width–size relation revealed by NH_3 , C^{18}O , ^{13}CO , and H I shows self-similar structure between 0.1 – 40 pc . Its slope is $\alpha = 0.41 \pm 0.06$.
- (vii) The typical size, kinetic temperature and line width of NH_3 cores rank L 1340 between the high mass star forming regions Perseus and Orion B, whereas its total mass is some two orders of magnitude smaller, and no high mass stars have been formed in it. Apparently most of the ISM around L 1340 is in the form of H I .

Acknowledgements. This research was supported by the Hungarian OTKA grants T022946, T024027, T034998,

T034584, and T037508. We also received support from the German–Hungarian Technological and Scientific Cooperation Project No. 121. L. V. T. acknowledges financial support from the Academy of Finland grant No. 174854. This research has made use of the USNOFS Image and Catalogue Archive operated by the United States Naval Observatory, Flagstaff Station (<http://www.nofs.navy.mil/data/fchpix/>). We thank to Péter Ábrahám and Attila Moór for their help in handling the H I data, and László Szabados for careful reading of the manuscript.

Appendix A: Distribution of the H I around L 1340

The angular resolution of the Leiden–Dwingeloo H I survey data is $0''.6$, corresponding to 6.3 pc at the distance of L 1340, and the velocity resolution is 1.03 km s^{-1} . Fig. A.1 shows the H I spectrum at $(130^{\circ}5, +11^{\circ}5)$, and in the velocity interval $-40\text{ km s}^{-1} < v_{\text{LSR}} < +10\text{ km s}^{-1}$. The peak at 0 km s^{-1} probably corresponds to the atomic cloud associated with the molecular cloud L 1333 located at a distance of 180 pc around $(l, b)=(128^{\circ}9, 13^{\circ}7)$, and at the same mean radial velocity (Obayashi et al. 1998). The

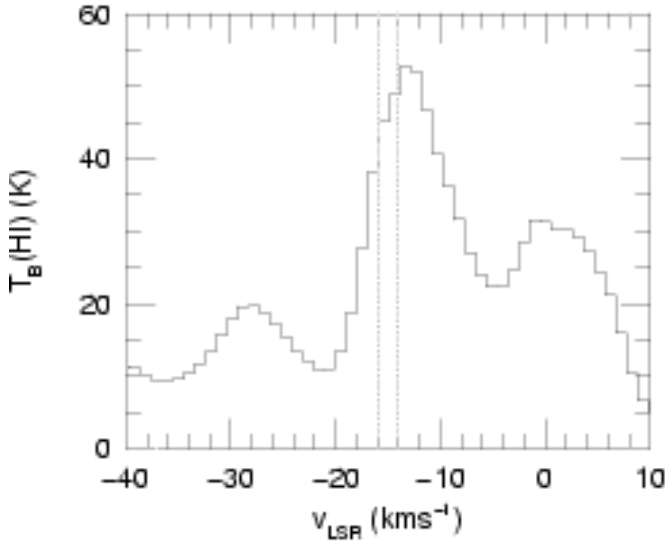


Fig. A.1. HI spectrum at $l = 130^{\circ}.5, b = +11^{\circ}.5$ taken from the Leiden–Dwingeloo survey. The angular resolution of the survey is $0^{\circ}.5$, and the spectral resolution is 1.03 km s^{-1} . Dotted vertical lines indicate the radial velocity range of the molecular cloud.

highest peak of the spectrum at $v_{\text{LSR}} = -13 \text{ km s}^{-1}$ represents the HI cloud enveloping L 1340. The characteristic line width of this spectral feature is $\sim 7 \text{ km s}^{-1}$.

Fig. A.2 shows the distribution of the neutral hydrogen integrated over the velocity interval $-18 \text{ km s}^{-1} < v_{\text{LSR}} < -8 \text{ km s}^{-1}$. A large, elongated HI structure can be seen in the area $126^{\circ} \leq l \leq 142^{\circ}$ and $+7^{\circ} \leq b \leq +13^{\circ}$ in this radial velocity interval. Its radius, derived from the area within the half-maximum contour, is $\sim 38 \text{ pc}$. The apparent local minimum in HI near the molecular cloud may result both from self-absorption and conversion of a part of hydrogen into molecules. The HI column densities displayed in Fig. A.2 were estimated assuming optically thin emission, i.e. using the relationship

$$N(\text{HI}) = 1.8224 \times 10^{18} \int T_b dv \text{ cm}^{-2} (\text{K km s}^{-1})^{-1} \quad (\text{A.1})$$

(Rohlfs & Wilson 2000). The mass of the HI structure, estimated via summing up the column densities inside the half-maximum contour is $M(\text{HI}) \geq 2 \times 10^4 M_{\odot}$, comparable with those of some well known nearby molecular cloud complexes (e.g. Taurus), and an order of magnitude larger than the mass of the molecular cloud.

Appendix B: Deriving the distribution of A_V from star counts

We used the USNOFS Image and Catalogue Archive to derive the distribution of the visual extinction A_V in a field of $1^{\circ} \times 1^{\circ}$ containing L 1340. We counted the stars on overlapping circles of $3'$ in diameter, the centres of which were distributed on a regular grid with step of $30''$. We

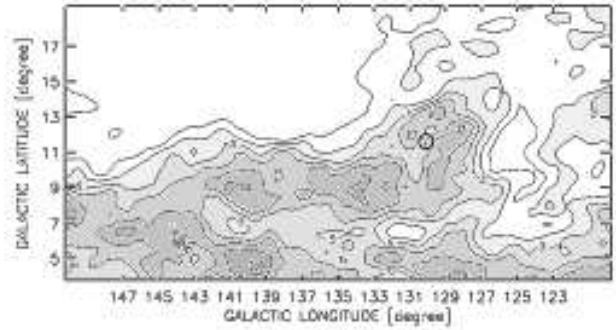


Fig. A.2. Distribution of the neutral hydrogen over a $30^{\circ} \times 15^{\circ}$ area including L 1340, integrated over the velocity interval $-18 \text{ km s}^{-1} < v_{\text{LSR}} < -8 \text{ km s}^{-1}$, taken from the Leiden–Dwingeloo survey. The only known molecular cloud in this area is L 1340, marked by the circle. Column densities were derived assuming optically thin emission. The lowest contour is at $3 \times 10^{20} \text{ cm}^{-2}$, and the increment is 10^{20} cm^{-2} .

removed from the stellar list all known candidate pre-main sequence stars associated with the cloud, and all identified foreground stars. We derived A_V from R star counts using the method described by Dickman (1978). The extinction-free reference area was a field $20' \times 20'$ centred on $\text{RA}(2000)=1^{\text{h}}52^{\text{m}}$, $\text{Dec}(2000)=+73^{\circ}15'$. A_V values obtained in this manner saturate at 6 mag.

We estimated the contribution of the foreground diffuse matter to A_V with the aid of the neutral hydrogen spectra (see Fig. A.1). Assuming optically thin radiation we used the relationship A.1 to derive hydrogen column densities from the spectra, and regarded as foreground all the HI gas at velocities $v_{\text{LSR}} > -6 \text{ km s}^{-1}$, as well as half of the gas at $-20 \text{ km s}^{-1} < v_{\text{LSR}} < -6 \text{ km s}^{-1}$. Taking the average of four HI spectra covering the face of L 1340, and using the relationship $N(\text{HI}) \approx 2 \times 10^{21} [\text{cm}^{-2}/\text{mag}] A_V$ (Spitzer 1978) we obtained $A_{V,f} \approx 0.55 \text{ mag}$ for the foreground extinction to be subtracted from the A_V values derived from the star counts.

References

- Adams F. C. & Myers P. C. 2001, ApJ 553, 744
- Assendorp R., Bontekoe T. R., de Jonge A. R. W. et al. 1995, A&S, 110, 395
- Baars J.W.M., Genzel R., Pauliny-Toth I. I. K. & Witzel A. 1977, A&A 61, 99
- Bergin E. A. & Langer W. D., 1997, ApJ 486, 316
- Bertoldi F. & McKee C. F. 1992, ApJ 395, 140
- Blitz L. & Williams J.P., 1999, The Origin of Stars and Planetary Systems, eds. C.J. Lada & N. D. Kylafis, Kluwer, p. 3
- Caselli P. & Myers P. C. 1995, ApJ 446, 665
- Cohen M. 1980, AJ, 85, 29
- Danby G., Flower D.R., Valiron P. et al. 1988, MNRAS 235, 229
- Dickman R. L., 1978, AJ 83, 363
- Dorschner J. & Gürtler J. 1966, AN 289, 65

- Elmegreen B. G. 1993, *ApJ* 419, L29
- Forveille T., Guilloteau S. & Lucas R., 1989, CLASS Manual Version 4.0
- Goodman A. A., Barranco J. A., Wilner D. J. & Heyer M. H. 1998, *ApJ* 504, 223
- Harju J., Walmsley C. M. & Wouterloot J.G.A. 1993, *A&AS* 98, 51 (HWW)
- Hartmann D. & Burton W. B. 1997, Atlas of Galactic Neutral Hydrogen, Cambridge Univ. Press
- Ho P. T. P. & Townes C. H. 1983, *ARA&A* 21, 239
- Jijina J., Myers P. C. & Adams F. C. 1999, *ApJS* 125, 161 (JMA)
- Klessen R. S., Heitsch F. & Mac Low M.-M. 2000, *ApJ* 535, 887
- Kumar M. S. N., Anandarao B. G. & Yu K. C. 2002, *AJ* 123, 2583
- Kun M. 2002a, in: Galactic Star Formation Across the Stellar Mass Spectrum, ASP Conf. Ser., in press
- Kun M. 2002b, in preparation
- Kun M., Obayashi A., Sato F. et al. 1994, *A&A* 292, 249 (Paper I)
- Larson R. B. 1981, *MNRAS* 194, 809
- Martin R. N. & Barrett A. H. 1978, *ApJS* 36, 1
- Mitchell G. F., Johnstone D., Moriarty-Schieven G., Fich M. & Tothill N. F. H. 2001, *ApJ* 556, 215
- Motte F., André P. & Neri R. 1998, *A&A* 336, 150
- Myers P. C. 1998, *ApJ* 496, L109
- Myers P. C., Fuller G. A., Mathieu R. D., et al. 1987, *ApJ* 319, 340
- Myers P. C. & Fuller G. A. 1993, *ApJ* 402, 635 773
- Nejad L. A. M., Williams D. A. & Charnley S. B., 1990, *MNRAS* 246, 183
- Obayashi A., Kun M., Sato F. et al. 1998, *AJ* 115, 274
- Padoan P. 1995, *MNRAS* 277, 377
- Padoan P. & Nordlund Å. 2002, *ApJ*, in press
- Rohlfs K. & Wilson T. L. 2000, Tools of Radio Astronomy, Springer, p. 308
- Spitzer L. 1978, Physical Processes in the Interstellar Medium, John Wiley & Sons, p. 156
- Suzuki H., Yamamoto S., Ohishi M. et al. 1992, *ApJ* 392, 551
- Tafalla M., Myers P. C., Caselli P. et al. 2002, *ApJ* 569, 815
- Testi L., Palla F., & Natta A. 1999, *A&A* 342, 515
- Walmsley C.M. & Ungerechts H. 1983, *A&A* 122, 164
- Wang T.Y., Wouterloot J. G. A. & Wilson T. L. 1993, *A&A* 277, 205
- Williams J. P., Blitz L. & McKee C. F. 2000, Protostars and Planets IV, eds. V. Mannings, A. P. Boss & S. S. Russell, Univ. of Arizona Press, p. 97
- Yonekura Y., Dobashi K., Mizuno A. et al. 1997, *ApJS* 110, 21